APPENDIX A

Lemma 1 (Local Optimality): For the control system of the acupuncture robot, if the parameters in L_{sp} and vel-con are appropriately selected, there exists $w^* > 0$ such that, for all $w > w^*$, the trajectory-constrained model predictive control (TCMPC) can be equivalently transformed into a constrained linear quadratic regulator (LQR), and it holds that:

$$\boldsymbol{u}_k = \arg\min_{\boldsymbol{u}\in\mathbb{U}} \; w\cdot\left\|T_s\boldsymbol{J}_{Tk}\boldsymbol{u}-\boldsymbol{S}_d\right\|^2 \tag{A.1}$$

Proof: With trajectory tracking included as a constraint, the standard MPC problem $P_N^r(\boldsymbol{\xi}, q_k^d)$ can be defined as follows:

$$\begin{aligned} V_N^{r*}(\boldsymbol{\xi},\boldsymbol{q}_k^d) &= \min_{\boldsymbol{\delta U}_k,\hat{\boldsymbol{q}}_k} \; L_{Sp} \\ &\text{s.t.} \quad \text{vel-con} \\ &\quad \mathrm{T}_s\boldsymbol{J}_k\boldsymbol{u}_k = \boldsymbol{S}_d \end{aligned} \tag{A.2}$$

Based on Eq. (A.2), the optimization problem can be further defined as $P_N^m(\boldsymbol{\xi},\boldsymbol{q}_k^d)$, which is expressed as:

$$\begin{aligned} V_{N,w}^{m*}(\boldsymbol{\xi},\boldsymbol{q}_k^d) &= \min_{\boldsymbol{\delta U}_k,\hat{\boldsymbol{q}}_k} \; L_{Sp} + w\left\|\Delta T\boldsymbol{J}_k\boldsymbol{u}_k-\boldsymbol{S}_d\right\|_1 \\ &\text{s.t.} \quad \text{vel-con} \end{aligned} \tag{A.3}$$

Building on [42], $\exists w^* > 0$, such that for any $w > w^*$, the condition $V_N^{m*}(\boldsymbol{\xi},\boldsymbol{q}_k^d) = V_N^{r*}(\boldsymbol{\xi},\boldsymbol{q}_k^d)$ holds for all variables within the feasible domain, and the following expression is obtained:

$$\boldsymbol{u}_k = \arg\min_{\boldsymbol{u}\in\mathbb{U}} w\cdot\left\|T_s\boldsymbol{J}_{Tk}\boldsymbol{u}-\boldsymbol{S}_d\right\|_1 \tag{A.4}$$

Let $w_2 > w_1 > w^*$. Based on the properties of convex functions, the following holds:

$$\begin{aligned} w_1\left\|T_s\boldsymbol{J}_k\boldsymbol{u}_k-\boldsymbol{S}_d\right\|_1 &\le w\left\|T_s\boldsymbol{J}_k\boldsymbol{u}_k-\boldsymbol{S}_d\right\|^2 \\ &\le w_2\left\|T_s\boldsymbol{J}_k\boldsymbol{u}_k-\boldsymbol{S}_d\right\|_1 \end{aligned} \tag{A.5}$$

Therefore:

$$V_{N,w_1}^{m*}(\boldsymbol{\xi},\boldsymbol{q}_k^d) \le V_N^{FS*}(\boldsymbol{\xi},\boldsymbol{q}_k^d) \le V_{N,w_2}^{m*}(\boldsymbol{\xi},\boldsymbol{q}_k^d) \tag{A.6}$$

Further:

$$V_N^{r*}(\boldsymbol{\xi},\boldsymbol{q}_k^d) \le V_N^{FS*}(\boldsymbol{\xi},\boldsymbol{q}_k^d) \le V_N^{r*}(\boldsymbol{\xi},\boldsymbol{q}_k^d) \tag{A.7}$$

Therefore, $V_N^{FS*}(\boldsymbol{\xi},\boldsymbol{q}_k^d) = V_N^{r*}(\boldsymbol{\xi},\boldsymbol{q}_k^d)$, and it follows that:

$$\boldsymbol{u}_k = \arg\min_{\boldsymbol{u}\in\mathbb{U}} w\cdot\left\|T_s\boldsymbol{J}_{Tk}\boldsymbol{u}-\boldsymbol{S}_d\right\|^2 \tag{A.8}$$

Theorem 1 (Stability): For the TCMPC of the acupuncture robot, with the selection of $\boldsymbol{Q}$, $\boldsymbol{R}$, $\boldsymbol{P}_{\mathrm{TC}}$, V, and $\mathbb{O}_\epsilon$ following Ref. [21], and given the target joint angle $\boldsymbol{q}_k^d$ and the target sequence $\boldsymbol{S}_d = [\boldsymbol{S}_{d1}, \boldsymbol{S}_{d2}, \ldots \boldsymbol{S}_{dn}]$ for trajectory tracking, if the final convergence direction of $\boldsymbol{S}_{dk}$ is aligned with $\boldsymbol{q}_k \to \boldsymbol{q}_k^d$, then:

1) If $\boldsymbol{q}_k^d \in \mathbb{Q}$ and $\boldsymbol{S}_d$ satisfy vel-con, the closed-loop system is asymptotically stable, and the target tracking conditions are always satisfied.
2) Otherwise, the closed-loop system is in an asymptotically stable state and satisfies:

$$\hat{\boldsymbol{q}}_k = \arg\min_{\boldsymbol{q}\in\boldsymbol{Q}} \left\|\boldsymbol{q}-\boldsymbol{q}_k^d\right\|_V^2 \tag{A.9}$$

Proof: The core of the proof involves demonstrating that the optimal value of the Lyapunov function decreases after incorporating $w\cdot\left\|T_s\bar{\boldsymbol{J}}_{Tk}\boldsymbol{u}_k-\boldsymbol{S}_d\right\|^2$. The proof strategy focuses on recursive feasibility and $\boldsymbol{\xi}_k$ convergence to 0, similar to the proof in Refs. [20][21][43]. Considering at time k, if the solution to Eq. (11) is $\left(\delta\boldsymbol{q}_{k|k}, \boldsymbol{q}_{k|k}, \hat{\boldsymbol{q}}_k^d, \delta\boldsymbol{u}_{[k:k+N-1]|t}\right)$, then a feasible solution at time $k+1$ is $\left(\delta\boldsymbol{q}_{k+1|k}, \boldsymbol{q}_{k+1|k}, \hat{\boldsymbol{q}}_k^d, \delta\boldsymbol{u}_{[k+1:k+N]|t}\right)$. $\delta\boldsymbol{u}_{k+N|t} = \kappa\boldsymbol{\xi}_{k+N|t}$ is consistent with the definition in Ref. [21]. Substitute the feasible solution at time $k+1$ into Eq. (11). According to Refs. [21][43], there is:

$$\begin{aligned} &V_{N|k+1}^{FS*}\left(\boldsymbol{\xi}_{k+1|k}, \delta\boldsymbol{u}_{[k+1:k+N]|k}\right) - V_{N|k}^{FS*}\left(\boldsymbol{\xi}_{k|k}, \delta\boldsymbol{u}_{[k:k+N-1]|k}\right) \\ &\le -\left\|\boldsymbol{\xi}_{k|k}\right\|_Q^2 - \left\|\delta\boldsymbol{u}_{k|k}\right\|_R^2 - w\cdot\left\|T_s\boldsymbol{J}_{k|k}\boldsymbol{u}_{k|k}-\boldsymbol{S}_{d|k}\right\|^2 \\ &\quad + w\cdot\left\|T_s\boldsymbol{J}_{k+1|k}\boldsymbol{u}_{k+1|k}-\boldsymbol{S}_{d|k+1}\right\|^2 \end{aligned} \tag{A.10}$$

When the trajectory tracking convergence direction of $\boldsymbol{S}_{d|k} \to \boldsymbol{S}_{d|k+n}$ is aligned with $\boldsymbol{q}_k \to \boldsymbol{q}_k^d$, which, in other words, the direction of trajectory tracking is consistent with the system approaching steady state, $\exists k^* > 0$, such that $\forall k > k^*$, there is:

$$\left\|\boldsymbol{S}_{d|k}\right\| > \left\|\boldsymbol{S}_{d|k+1}\right\| > \left\|\boldsymbol{S}_{d|k+2}\right\| > \ldots \tag{A.11}$$

According to optimality, there is:

$$\begin{aligned} &V_{N|k+1}^{FS*}\left(\boldsymbol{\xi}_{k+1|k}, \delta\boldsymbol{u}_{[k+1:k+N]|k}\right) - V_{N|k}^{FS*}\left(\boldsymbol{\xi}_{k|k}, \delta\boldsymbol{u}_{[k:k+N-1]|k}\right) \\ &\le -\left\|\boldsymbol{\xi}_{k|k}\right\|_Q^2 - \left\|\delta\boldsymbol{u}_{k|k}\right\|_R^2 - \min_{\boldsymbol{u}_k\in\mathbb{U}} w\cdot\left\|T_s\boldsymbol{J}_{k|k}\boldsymbol{u}_{k|k}-\boldsymbol{S}_{d|k}\right\|^2 \\ &\quad + \min_{\boldsymbol{u}_{k+1}\in\mathbb{U}} w\cdot\left\|T_s\boldsymbol{J}_{k+1|k+1}\boldsymbol{u}_{k+1|k+1}-\boldsymbol{S}_{d|k+1}\right\|^2 \end{aligned} \tag{A.12}$$

If $\boldsymbol{S}_{d|k} / (T_s J_{k|k}) \in \mathbb{U}$, then according to ***Lemma 1***, the following holds:

$$T_s\boldsymbol{J}_{k|k}\boldsymbol{u}_{k|k} = \boldsymbol{S}_{d|k} \tag{A.13}$$

Therefore:

$$\min_{\boldsymbol{u}_k\in\mathbb{U}} w\cdot\left\|T_s\boldsymbol{J}_{k|k}\boldsymbol{u}_{k|k}-\boldsymbol{S}_{d|k}\right\|^2 = 0 \tag{A.14}$$

According to Eq. (A.11), $\boldsymbol{S}_{d|k+1} / (T_s\boldsymbol{J}_{k+1|k+1}) \in \mathbb{U}$ also holds true, so:

$$\min_{\boldsymbol{u}_{k+1}\in\mathbb{U}} w\cdot\left\|T_s\boldsymbol{J}_{k+1|k+1}\boldsymbol{u}_{k+1|k+1}-\boldsymbol{S}_{d|k+1}\right\|^2 = 0 \tag{A.15}$$

If $\boldsymbol{S}_{d|k} / (T_s\boldsymbol{J}_{k|k}) \notin \mathbb{U}$, then $\min_{\boldsymbol{u}_k\in\mathbb{U}} w\cdot\left\|T_s\boldsymbol{J}_{k|k}\boldsymbol{u}_{k|k}-\boldsymbol{S}_{d|k}\right\|^2$ represents the distance between $\boldsymbol{S}_{d|k}$ and the feasible domain. Based on Eq. (A.11) and ***Lemma 1***, the distance between $\boldsymbol{S}_{d|k+1}$ and the feasible domain is less than $\boldsymbol{S}_{d|k}$, that is:

$$\min_{\boldsymbol{u}_k\in\mathbb{U}} w\cdot\left\|T_s\boldsymbol{J}_{k|k}\boldsymbol{u}_{k|k}-\boldsymbol{S}_{d|k}\right\|^2 > \min_{\boldsymbol{u}_{k+1}\in\mathbb{U}} w\cdot\left\|T_s\boldsymbol{J}_{k+1|k+1}\boldsymbol{u}_{k+1|k+1}-\boldsymbol{S}_{d|k+1}\right\|^2 \tag{A.16}$$

In summary, the following inequality always holds true under the assumption:

$$\begin{aligned} &-\min_{\boldsymbol{u}_k\in\mathbb{U}} w\cdot\left\|T_s\boldsymbol{J}_{k|k}\boldsymbol{u}_{k|k}-\boldsymbol{S}_{d|k}\right\|^2 \\ &\quad + \min_{\boldsymbol{u}_{k+1}\in\mathbb{U}} w\cdot\left\|T_s\boldsymbol{J}_{k+1|k+1}\boldsymbol{u}_{k+1|k+1}-\boldsymbol{S}_{d|k+1}\right\|^2 \le 0 \end{aligned} \tag{A.17}$$

Consequently:

$$V_{N|k+1}^{FS*}\left(\boldsymbol{\xi}_{k+1|k},\delta\boldsymbol{u}_{[k+1:k+N]|k}\right) - V_{N|k}^{FS*}(\boldsymbol{\xi}_{k|k},\delta\boldsymbol{u}_{[k:k+N-1]|k}) < 0 \tag{A.18}$$

Eq. (A.18) holds true for $\forall k > k^*$, thus concluding the proof of ***Theorem 1***.

APPENDIX B

The control method using Eq. (9) to track the same right-angle trajectories shows significant dependence on the segmentation tracking precision and exhibits poor adaptability to different trajectories. Setting the initial point to (45, 97, 67)mm and extracting target points 1 and 2, with segmentation intervals of 5 mm, 15 mm, and 50 mm, and joint angle error thresholds for segmentation switches set to 1e-1, 1e-2, and 1e-3, respectively, the corresponding simulation results are shown in **Fig. B.1**. It can be observed that segmentation precision affects the differences of $\boldsymbol{q}_k^d$ between segments. When the higher segmentation precision is required, the switching threshold needs to be set to a reasonably small value, but it should not be too small, otherwise, switching to the next segment will be impossible. Conversely, with lower segmentation precision, the switching threshold should be set to a reasonably large value. Additionally, the controller shows poor adaptability to different tracking trajectories. The optimal parameters for tracking trajectory 1 perform poorly for tracking trajectory 2. In summary, without explicitly incorporating Cartesian trajectory tracking constraints, the control method based on Eq. (9) exhibits extremely poor robustness for tracking specific trajectories of the acupuncture robot.

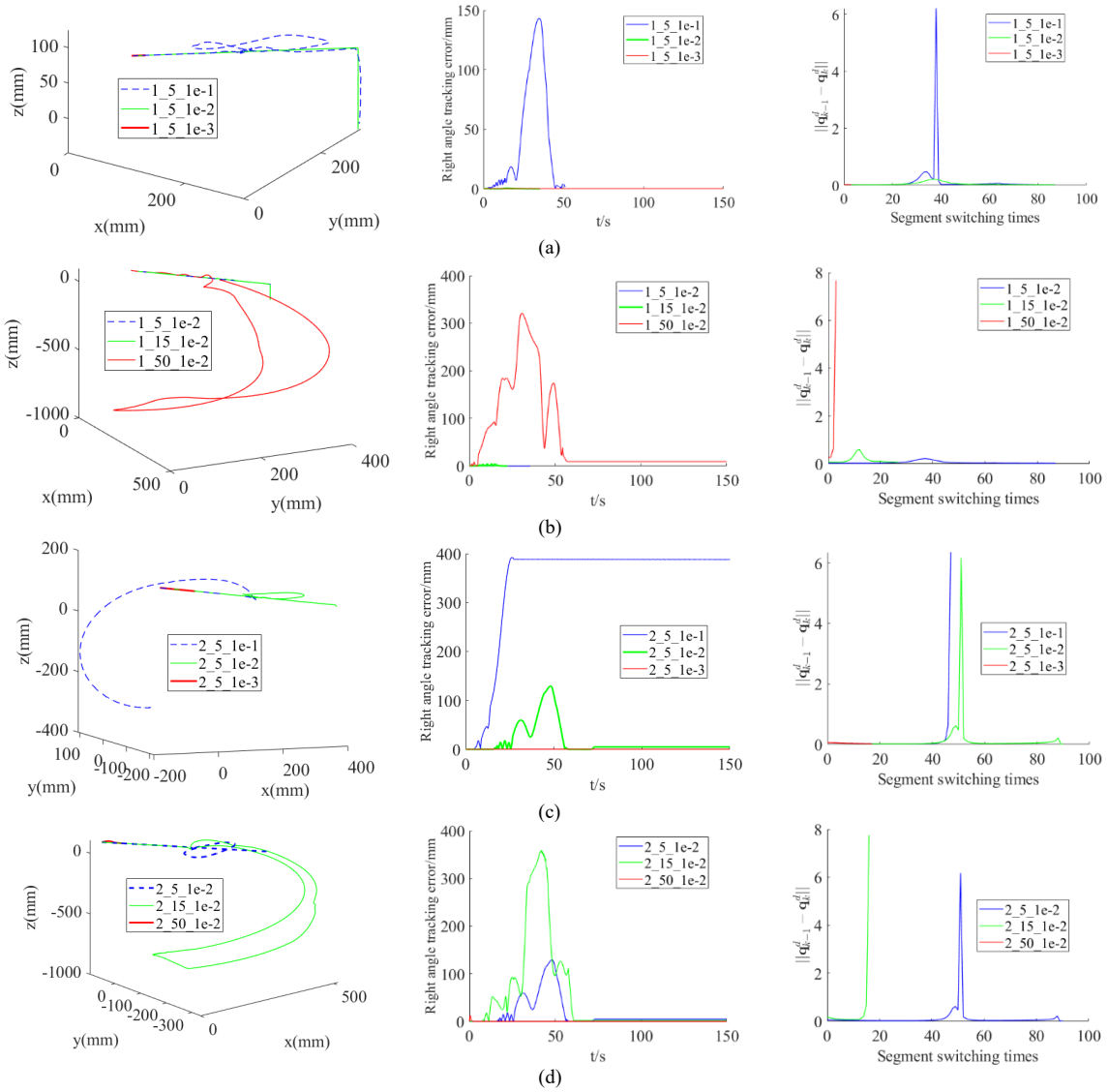

Fig. B.1 Tracking results of traditional MPC method. (a) Comparsion of target 1 with segment 5mm and different switching thresholds. (b) Comparsion of target 1 with switching threshold 1e-2 and different segments. (c) Comparsion of target 2 with segment 5mm and different switching thresholds. (d) Comparsion of target 2 with switching threshold 1e-2 and different segments.

Algorithm C.1 Right angle trajectory tracking method with dual camera acupoint location

Input: P_0 , P_k - initial and current end point , ${}^{G_C}O$, ${}^{L_C}O$ - acupoint located by global camera and hand-eye camera, O - acupoint from the last control sequence, ϵ - section switching threshold, $\boldsymbol{q}_{k-1}$, $\boldsymbol{q}_k$ - joint angle at the last and current control sequence, $\boldsymbol{u}_{k-1}$ - joint velocity at the last control sequence, flag - label of the right angle section

Output: $\boldsymbol{u}_k$ - joint velocity of the current control sequence, P_0 - updated initial end point, O - updated acupoint, flag

if ${}^{L_C}O$ is not none

$O \leftarrow {}^{L_C}O$;

else if ${}^{G_C}O$ is not none

$O \leftarrow {}^{G_C}O$;

end

$\boldsymbol{q}_k^d \leftarrow$ Eq. (5) and Eq. (3) with O ;

if $\|\boldsymbol{P}(x,y,z) - \boldsymbol{W}(x,y,z)\|_2 < \epsilon$ and flag is 1

Switch tracking section of the right-angle trajectory with flag $\leftarrow 0$

if $\|\boldsymbol{P}(x,y) - \boldsymbol{O}(x,y)\| > \epsilon$ and flag is 0

Restart the trajectory tracking with $\boldsymbol{P}_0(x,y,z) \leftarrow \boldsymbol{P}(x,y,z)$ and flag $\leftarrow 1$;

$\boldsymbol{W}(x,y,z) \leftarrow [O(x), O(y), P(z)]^{\mathrm{T}}$;

if flag is 1

$P_h = \text{Projection}(P, \overrightarrow{\mathrm{P_0T_0}})$;

$\boldsymbol{S}_d \leftarrow$ Eqs. (14), (16) and (17) with P_h , P_0 , W ;

else

$P_v = \text{Projection}(P, \overrightarrow{\mathrm{TO}})$,

$\boldsymbol{S}_d \leftarrow$ Eqs. (15), (16) and (17) with P_v , P_0 , W ;

end

$\boldsymbol{u}_k \leftarrow$ Eq. (18) with $\boldsymbol{q}_k^d$, $\boldsymbol{q}_{k-1}$, $\boldsymbol{q}_k$, $\boldsymbol{u}_{k-1}$ and $\boldsymbol{S}_d$

return $\boldsymbol{u}_k$, $\boldsymbol{P}_0$, O

Algorithm C.2 Sphere trajectory tracking method with force-bending perception

Input: P - center of the sphere, P' - tracking point, $\hat{\boldsymbol{F}}_s$ - force vector, r – sphere radius, $\boldsymbol{q}_{k-1}$, $\boldsymbol{q}_k$ - joint angle at the last and current control sequence, $\boldsymbol{u}_{k-1}$ - joint velocity at the last control sequence

Output: $\boldsymbol{u}_k$ - joint velocity of the current control sequence

${}^0\boldsymbol{p}_{\mathrm{H}} \leftarrow$ Eqs. (19) ~ (23) with P , P' , $\hat{\boldsymbol{F}}_s$ and r

Bending aware through $\theta \leftarrow \arccos\left(\dfrac{\overrightarrow{\mathrm{PP'}} \cdot \overrightarrow{\mathrm{PH}}}{\|\overrightarrow{\mathrm{PP'}}\| \|\overrightarrow{\mathrm{PH}}\|}\right)$ with P , P' and ${}^0\boldsymbol{p}_{\mathrm{H}}$

$\boldsymbol{q}_k^d \leftarrow$ Eqs. (24) ~ (25) with θ and ${}^0\boldsymbol{p}_{\mathrm{H}}$

Project P' to its sphere point $P'_r \leftarrow$ Eq. (26) with P , P' and r

$\boldsymbol{S}_d \leftarrow$ Eqs. (27) ~ (28) with P'_r , P' , ${}^0\boldsymbol{p}_{\mathrm{H}}$, θ and r

$\boldsymbol{u}_k \leftarrow$ Eq. (29) with $\boldsymbol{q}_{k-1}$, $\boldsymbol{q}_k$, $\boldsymbol{u}_{k-1}$, $\boldsymbol{q}_k^d$ and $\boldsymbol{S}_d$

return $\boldsymbol{u}_k$

APPENDIX C

The detailed implementation of the trajectory planning and tracking control method based on multiple sensor perception is shown in the following algorithm, with **Algorithm C.1** correspond to the rough positioning stage and **Algorithm C.2** correspond to the accurate positioning stage.

APPENDIX D

In the experimental system, the D-H parameters of the 8-DOF robot are shown in **TABLE D.1**.

TABLE D.1 The DH parameter of the 8-DOFAcuRobot

Joint	θ /°	d /mm	a /mm	α /°	Variable boundary
1	q_1	192.5	0	90	[-360, 360] /°
2	$q_2 + 90$	0	266	180	[-135, 135] /°
3	$q_3 + 90$	0	0	90	[-150, 150] /°
4	q_4	324	0	-90	[-360, 360] /°
5	q_5	0	0	90	[-147, 147] /°
6	q_6	155	0	0	[-360, 360] /°
7	0	$q_7 + 45$	0	0	[0, 50] mm
8	q_8	250	36.12	0	[-360, 360] /°

APPENDIX E

Different bending situations of the needle under different environment and position circumstances are explored. The bending degree and orientation with the corresponding ${}^{\mathrm{E}}\boldsymbol{F}_s$ are shown in **Fig. E.1.**

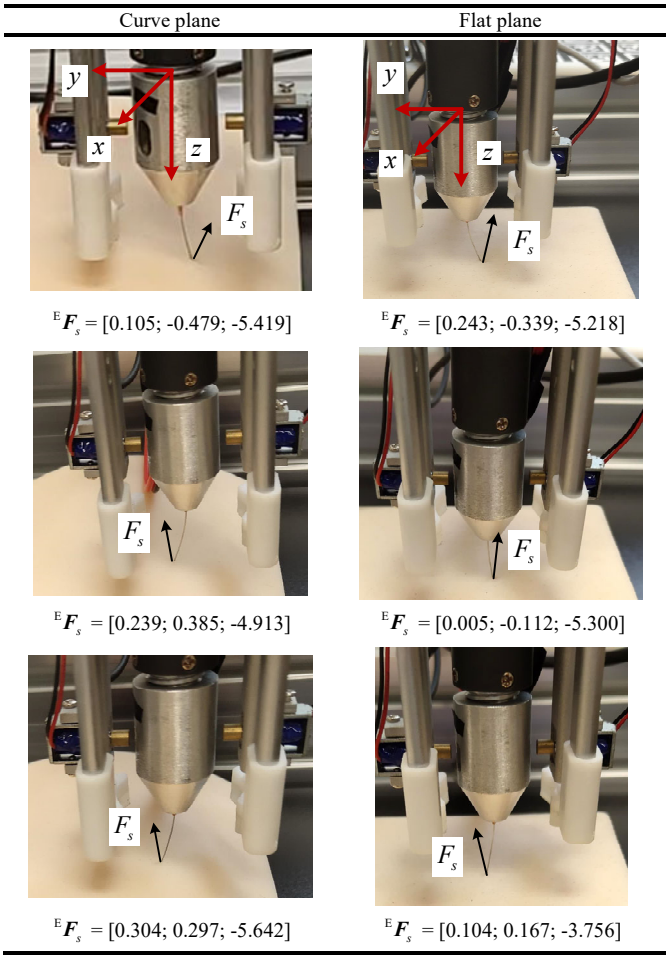

Fig. E.1 Force and bending degree of needle tip on flat and curved tissues